WILEY VCH

RESEARCH ARTICLE

Rational Design of a Robust Microporous Hydrogen-Bonded Organic Framework for Selective Gas Sorption

Manuel Carrera,[a] Ion Such-Basáñez,[b] Juan Pablo Marco-Lozar,[c] Agustín Bueno-López,[d] Eduardo Vilaplana-Ortego,[d] Iván da Silva,[e] Delia Bautista,[f] Alberto Fernández-Alarcón,[g] Joaquín Calbo,[g] Enrique Ortí,[g] David Curiel*[a]

[a] Dr. M. Carrera, Prof. D. Curiel
Department of Organic Chemistry – Faculty of Chemistry
University of Murcia
30100-Murcia (Spain)
E-mail: davidcc@um.es

[b] Dr. I. Such-Basáñez
Technical Research Services (SSTTI)
University of Alicante
Parque Científico, 03690 Sant Vicent del Raspeig, Alicante (Spain)

[c] Dr. J. P. Marco Lozar
Gas to Materials Technologies S. L.
c/ El Martillo, 7, 03690 Sant Vicent del Raspeig, Alicante (Spain)

[d] Dr. A. Bueno-López, B.Sc. E. Vilaplana-Ortego
Department of Inorganic Chemistry – Faculty of Science
University of Alicante
03690 Sant Vicent del Raspeig, Alicante (Spain)

[e] Dr. I. da Silva
ISIS Neutron and Muon Source
STFC Rutherford Appleton Laboratory
Chilton, Oxfordshire, OX110QX (United Kingdom)

[f] Dr. D. Bautista
Scientific Instrumentation Services
University of Murcia
30100-Murcia (Spain)

[g] Dr. D. A. Fernández-Alarcón. Dr. J. Calbo, Prof. E. Ortí
Institute of Molecular Science
University of Valencia,
Catedrático José Beltrán 2, 46980 Paterna (Spain)

Supporting information for this article is given via a link at the end of the document.((Please delete this text if not appropriate.))

Abstract: 7-Azaindole has been integrated as building block with complementary N-H···N hydrogen bonding sites for the synthesis of a tetrahedral molecular tecton, namely tetra(α-carbolin-6-yl)methane, TACM. The self-assembly of this molecule results in a 3D hydrogen-bonded organic framework (HOF). This supramolecular structure constitutes a crystalline microporous material with an extraordinary thermal and chemical robustness. Single crystal X-ray diffraction reveals how the five-fold catenation of diamonoid systems, stabilized by hydrogen bonds and π-π interactions, form an interpenetrated network with monodimensional channels. The structural features of the crystalline material are also observed by transmission electron microscopy (TEM). Additionally, the microporosity of the activated TACM-HOF is characterized by gas sorption (N_2, CO_2, CH_4 and H_2) experiments performed at different pressures. A selective adsorption is observed for CO_2 uptake and TACM-HOF also presents a good adsorption capacity for H_2 among supramolecular organic frameworks.

Introduction

The advent of reticular chemistry[1] triggered the research about a novel class of crystalline porous materials, namely Metal Organic Frameworks (MOFs)[2] and Covalent Organic Frameworks (COFs),[3] revitalizing the study of porous materials traditionally represented by zeolites or active carbon materials. One of the most significant features of MOFs and COFs is their structural composition based on organic building blocks, linked together by coordinate and covalent bonds, respectively. Therefore, the

versatility of organic synthesis and coordination chemistry open up an infinite variety of structures that could be adapted to the requirements of the reticular material for any specific application.

Recently, a supramolecular approach for the development of crystalline porous materials has also gained relevance. In contrast to MOFs and COFs, the assembly of organic building blocks can also be achieved by non-covalent interactions. In this regard, hydrogen bonding has mainly constituted the driving force for the emergence of hydrogen-bonded organic frameworks (HOFs).[4] As expected, the weakness of hydrogen bonds, when compared to coordinate and covalent bonds, has represented an important challenge for the progress of HOFs. One of the main difficulties behind the slower development of these materials is related to the collapse of the hydrogen-bonded network during the activation process, i.e., in the course of removing the guest species occluded during the synthesis, mostly solvent molecules, to obtain the porous framework. Nevertheless, a thoughtful design of building blocks has successfully contributed to the target of achieving hydrogen-bonded organic frameworks with permanent porosity.[5] A compromise between the molecular rigidity and the directionality of hydrogen bonding sites is very important to obtain robust enough supramolecular frameworks. Additionally, the involvement of π-π stacking, ionic interactions or network interpenetration have become useful tools for the stabilization of HOFs.[6] With the development of non-covalent organic frameworks, the advantages of supramolecular chemistry, such as dynamic equilibrium, cooperativity or self-healing ability, can be incorporated into the reticular materials to optimize their properties. The adaptation of the porosity, surface area and functionalization of the framework has led to an outstanding expansion of their application in areas as diverse as catalysis, gas adsorption and separation, sensing, electronics, proton conductivity or biomedicine.[4d, 7]

As it has just been mentioned, the design of the molecular unit whose self-assembly will produce the growth of the HOF has to consider several aspects. Regarding the structure of the rigid core that will define critical features of the HOF such as geometry, pore size, rotational freedom or orientation of hydrogen bonding sites, a plethora of skeletons have been investigated (Figure 1). To mention a few, it is worth highlighting the use of triaryl or tetraaryl-substituted conjugated cores (benzene,[8] pyrene,[9] triphenylene,[10] hexazatrinaphthylene,[11] porphyrin,[12] tetraphenylethene,[13] tetrathiafulvalene,[14] etc.) or multibranched systems such as trypticene[15] or tetraphenylmethane,[16] among others.

Concerning the hydrogen bonding sites, the use of structures with self-complementarity between hydrogen bond donor and hydrogen bond acceptor sites represents one of the basic design rules for HOFs (Figure 1). In agreement with this principle, the natural dimerization of carboxylic acids (C=O···H-O) has made these groups the most studied function in planar and non-planar frameworks since the first reported examples of hydrogen bonded porous materials until present.[17] Nitrogen-based functional groups have also been used as hydrogen bonding motifs exploring diverse structures. The directionality of the N-H···O=C interaction has been elegantly explored through the constriction of the hydrogen bonding sites in heterocyclic structures such as pyridone and imidazolone.[15, 18] Diaminotriazine is another useful building block that has been attached to different rigid cores to exploit its multiple N-H···N interactions.[19] This kind of interaction has also been implemented through the incorporation of pyrazole and imidazole rings into the molecular unit to assemble.[20] Additionally, inspired by biological systems, supramolecular organic frameworks stabilized by the formation guanine-based hydrogen bonded G-cuadruplexes have been reported.[21]

Within this context, we have recently reported the utility of 7-azaindole as reciprocal hydrogen bond-directing building block. The integration of this unit into expanded polyheteroaromatic systems has enabled the control of unidirectional self-assembly and subsequent π-stacking of organic semiconductors.[22] Additionally, the synthesis of conjugated tripodal systems incorporating the 7-azaindole substructure has been used in the investigation of hydrogen-bonded 2D-materials.[23] It is worth highlighting that one of the important features of these supramolecular materials is their thermal robustness.

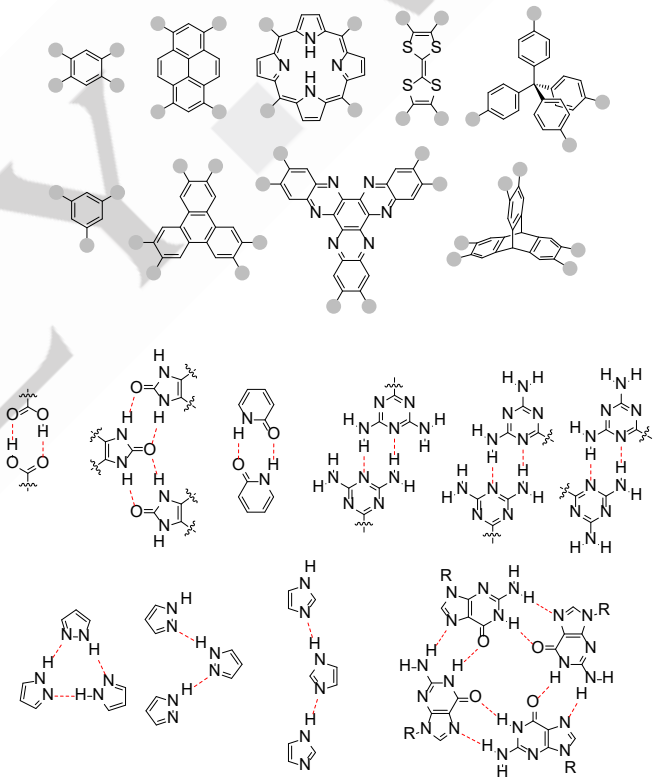

Figure 1. Building blocks (top) and hydrogen bonding groups (bottom) commonly employed for the design of HOFs.

Based on these precedents, we have designed a molecule that combines the abovementioned design rules, namely, the self-complementary hydrogen bonding ability of 7-azaindole, the rigidity resulting from the expansion of the conjugated system into an α-carboline, and the formation of a tetrahedral skeleton with the suitable orientation to self-assemble into a robust 3D-HOF. The tetra(α-carbolin-6-yl)methane, TACM-HOF, constitutes a microporous crystalline material that presents an interpenetrated

diamonoid network with monodimensional channels and an extraordinary robustness. This material shows interesting gas adsorption properties with selective uptake of CO_2 over CH_4 and significant H_2 capacity that highlight its performance within the context of emerging HOFs.

Results and Discussion

Synthesis and Structural Characterization

The synthesis of the tetra(α-carbolin-6-yl)methane is depicted in Scheme 1. It involved the nitration of tetraphenylmethane to isolate tetrakis(*p*-nitrophenyl)methane.[24] Then, nitro groups were reduced to subsequently perform a quadruple *N*-arylation with 2,3-dichloropyridine under Buchwald-Hartwig conditions. Finally, the cyclization through an intramolecular cross-coupling reaction, in each of the four branches, led to the α-carboline substructures of TACM. All the intermediate and final products were characterized by NMR and mass spectrometry. The experimental and spectroscopic details are provided in the Supporting Information (Figure S1–S9).

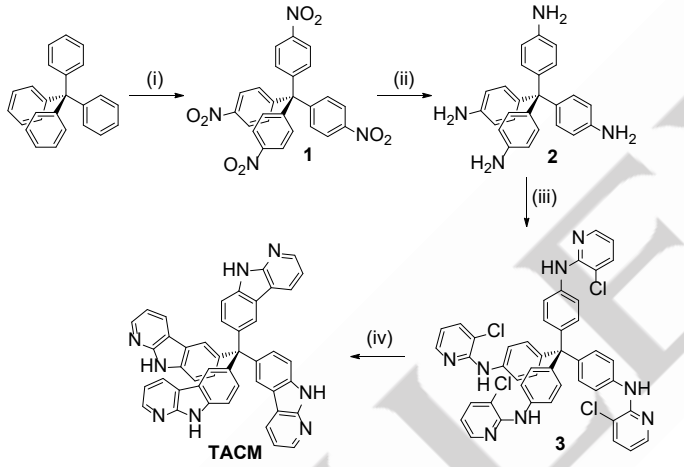

Scheme 1. Synthesis of TACM. (i) HNO_3 (fuming), Ac_2O, AcOH; (ii) H_2, Pd-C, MeOH; (iii) 2,3-dichloropyridine, $Pd(OAc)_2$, *rac*-BINAP, K_2CO_3, 1,4-dioxane, Δ; (iv) $Pd(dba)_2$, $PCy_3{\cdot}HBF_4$, DBU, 1,4-dioxane, Δ (sealed tube).

Single crystals of TACM were grown by slowly cooling down a 1,4-dioxane solution. Single-crystal X-ray diffraction experiments revealed that the molecule crystallizes in the I41/a space group (Figure 2 and 3). Disordered solvent molecules were occluded in the crystal network with an approximate occupancy of one molecule of dioxane per molecule in the unit cell (Figure S10). In any case, the disordered solvent has not been considered for the structure discussion. All the 7-azaindole units self-assemble through reciprocal N-H···N hydrogen bonds between the adequately oriented pyrrole and pyridine rings (2.86 Å N···N distance). Each tetrahedral molecule presents hydrogen bonding with four neighbor molecules setting edge-to-edge interactions between the α-carboline system. Additionally, each molecule has short contacts C-H···π (2.83 Å) and π-π (3.53 Å) with neighbor α-carboline units pointing in opposite directions (Figure 2 and 3a). Overall, these interactions contribute to the stabilization of the molecular packing.

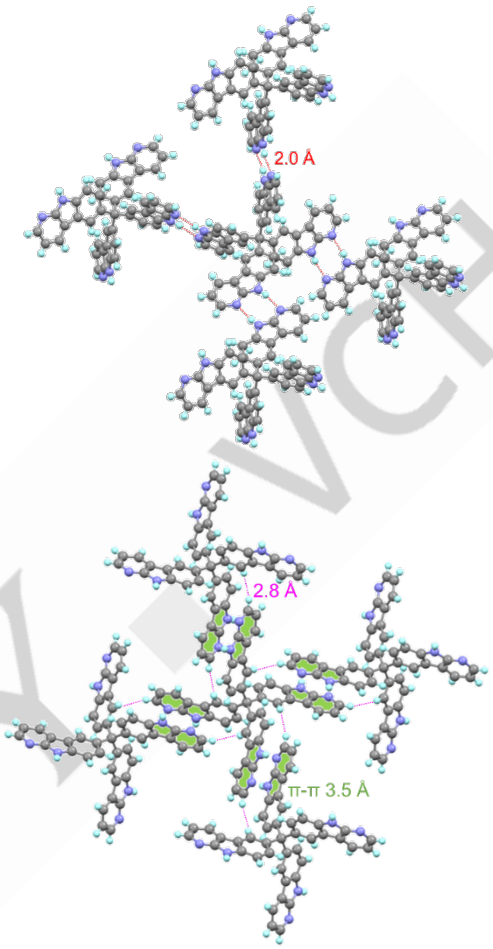

Figure 2. (Top) Hydrogen bond interactions (red dotted lines) in crystal packing; (Bottom) CH···π interactions (pink dotted lines) and π-stacked structures (green colored rings) in crystal packing.

The expansion of the hydrogen-bonded crystal network reveals the formation of distorted diamond-like cages whose dimensions are depicted in Figure 3b. When linking the sp^3 carbon atoms, the vertices of the four hexamers forming the diamonoid structure can be visualized. These supramolecular cages pack trough π-π interactions and form catenane motifs leading to five-fold interpenetrated networks (Figure 3d). On the whole, the hydrogen bonded organic framework defines helical channels along the c axis (Figure 4). Interestingly, right-handed helicity and left-handed helicity alternate between neighbor channels. The void volume of the unit cell is 27% (1103 $Å^3$) considering a probe radius of 1.2 Å and an approximate grid spacing of 0.2 Å,[25] calculated as the contact surface using Mercury software,[26] which corresponds to a solvent accessible surface of 6% (249 $Å^3$) (Figure S8). The cross-sectional view of the channel (Figure 4a) shows that the shortest and longest diagonals of the accessible pore have approximate dimensions of 0.49 and 0.66 nm, respectively.

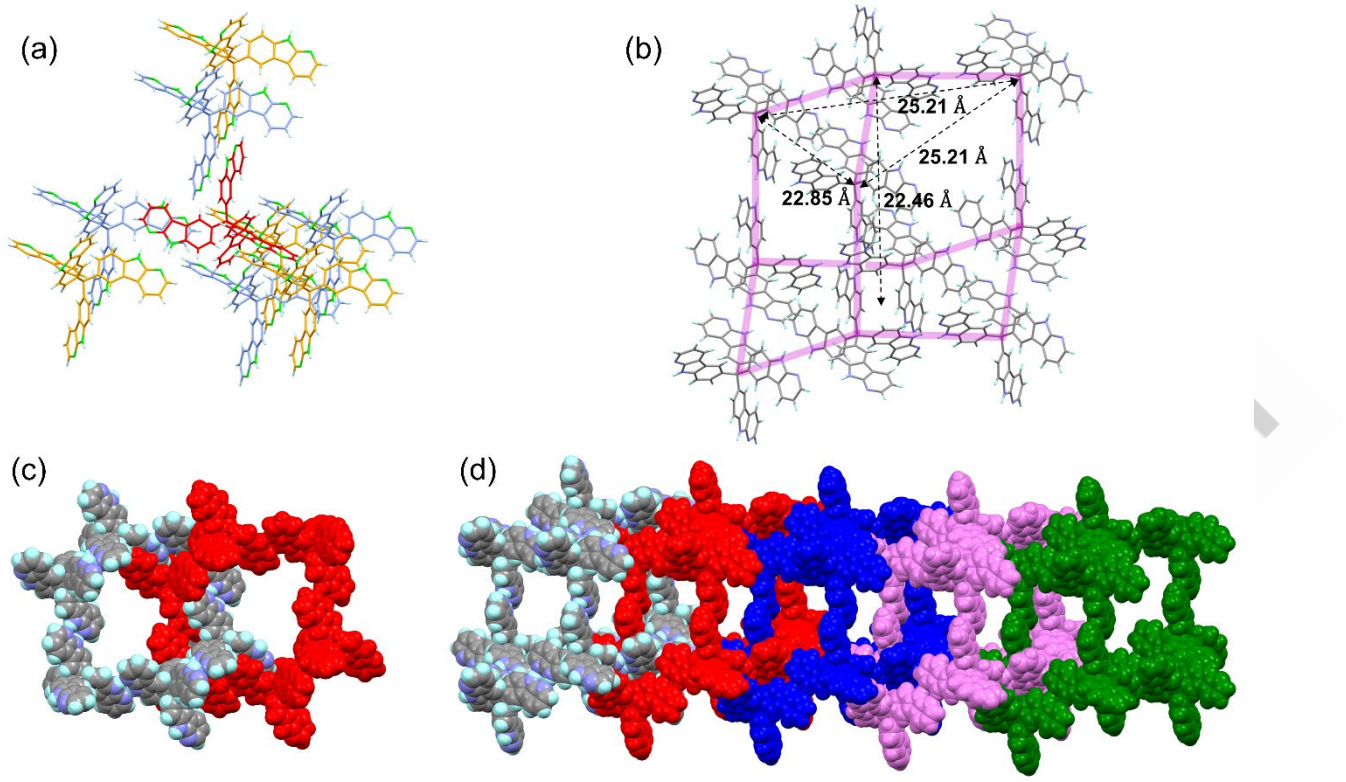

Figure 3. (a) Crystal packing of TACM. The red molecule is used as a reference to define intermolecular short contacts. This molecule is hydrogen-bonded to four neighbor molecules represented in yellow. Blue molecules set π-π interactions with each of the α-carboline units constituting the four branches of the tetrahedral red molecule. (b) Diamond-like structure constituted by hydrogen-bonded cyclic hexamers. (c) Simplified view of catenated hydrogen-bonded cyclic hexamers. (d) Five-fold interpenetrated diamond-like structures.

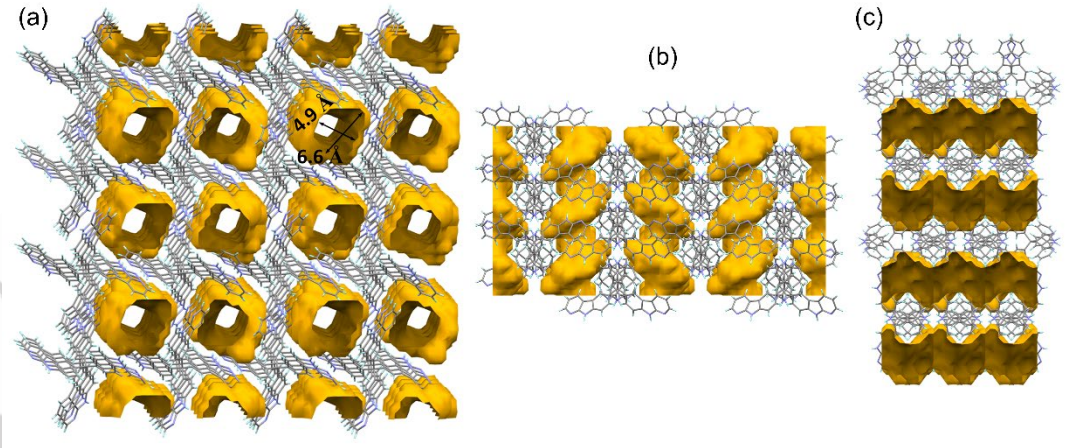

Figure 4. (a) Expanded crystal network with a perspective view of the channels across the c axis; (b) Helical channels observed by projecting the expanded crystal network across the a axis. (c) Cross section of the channels observed by projecting the expanded crystal network across the b axis.

The thermal robustness of the TACM framework was corroborated by thermogravimetric analysis. The crystalline solid was heated to remove the occluded solvent molecules and the weight percentage vs. temperature plot revealed a first step, at temperatures below 200ºC, corresponding to the mass loss (13.9%) assigned to the solvent evaporation. Subsequently, the abrupt change ascribed to the material decomposition started at a temperature as high as 515ºC. Differential scanning calorimetry measurements did not show any evidence of phase transitions after scanning several cycles (Figure S6).

Thermal stability was further investigated by X-ray diffraction (XRD) recorded after thermal treatments in air at

increasing temperatures (Figure 5a). The powder diffraction patterns show the characteristic TACM-HOF diffraction peaks until 350ºC, indicating that the framework did not collapse and maintained its crystallinity degree when heated. There are no new peaks arising from impurity phases and only subtle changes in the relative peak intensities are observed after heating, due to the structural change after removal of the occluded solvent molecules. The collapse of the structure occurs between 350 and 400 ºC, since the crystalline fingerprint totally disappeared after 400 ºC thermal treatment. Note that the mass changes in thermogravimetric analysis were monitored under heating ramp, while XRD in Figure 5a were recorded after 1 hour in isothermal conditions, which would explain the differences in the thermal stability threshold deduced from both techniques.

The chemical stability was also analyzed by XRD after immersion of TACM-HOF in different organic solvents (dichloromethane, acetone and toluene) and neutral, acidic or basic aqueous environment for 24 hours at room temperature (Figure 5b). XRD confirmed the chemical stability under all the chemical environments studied.

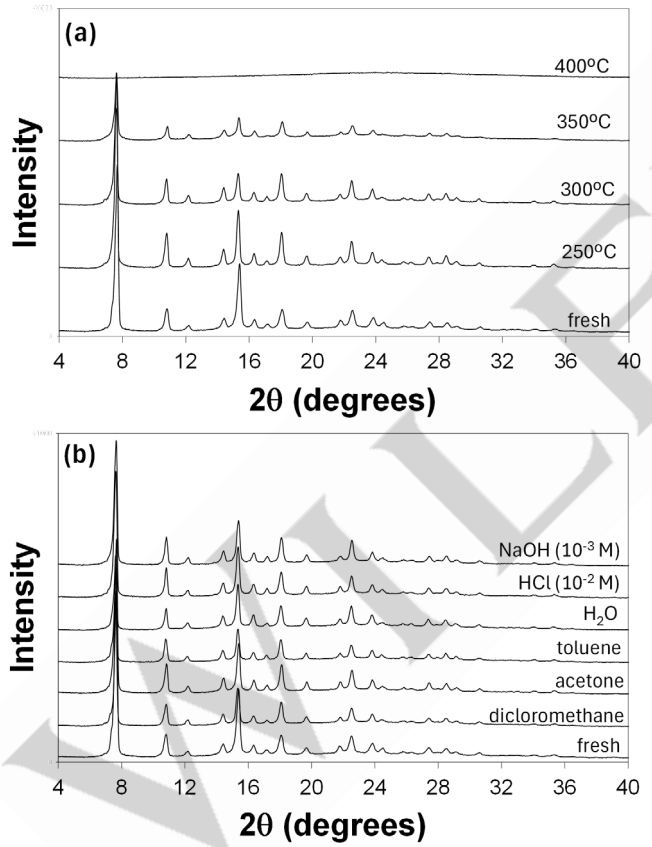

Figure 5. Powder X-ray diffraction of TACM-HOF (a) after thermal treatments in air at different temperatures for 1 hour and (b) after 24 hours immersed in different chemical environments.

An additional proof of the TACM-HOF stability was provided by the high-resolution transmission electron microscopy (HRTEM) measurements performed on the crystalline powder. Despite the known sensitivity of organic frameworks to the electron beam,[27] measurements performed at 200 kV offered good contrast for imaging. The HRTEM images confirmed the crystallinity of the porous structure of the particles where parallel planes could be resolved (Figure 6).

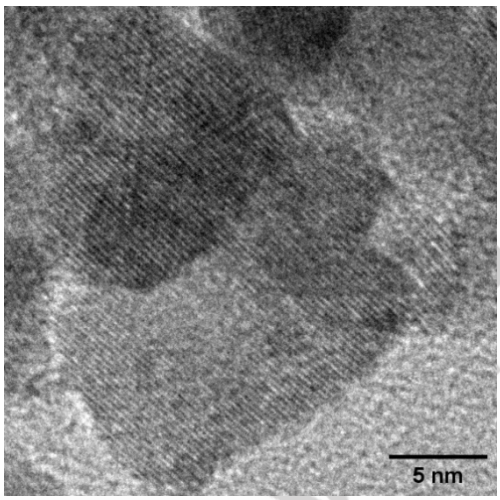

Figure 6. HRTEM image of TACM-HOF.

Textural Characterization and Gas Adsorption

Porous texture characterization of TACM-HOF was assessed by physical gas adsorption of N_2 and CO_2 at 77 K and 273 K, respectively. Concerning N_2 adsorption (Figure 7a), the plot corresponds to a type I isotherm with a narrow knee indicative of a homogeneous microporous (<2 nm) network system.[28] The isotherm reaches a plateau at low relative pressure, denoting an insignificant presence of mesopores (2-50 nm in diameter), with a very slight H4 hysteresis loop. A rise of the adsorption is also observed at pressures close to the saturation pressure. This increase could be due to the presence of interparticle voids or condensation on open surface, not related to the porous system of the TACM-HOF material.[29] The apparent Brunauer-Emmett-Teller (BET) surface area was estimated by fitting the experimental data to the BET equation following the Rouquerol rules,[28] and showed a value of 580 m^2g^{-1}. Complementary characterization of narrow microporosity (i.e. pore width < 0.7 nm) can be obtained from subatmospheric pressure CO_2 adsorption at 273 K.[30] In agreement with this, the subatmospheric region in the CO_2 isotherm (Figure 7b) reveals the presence of very narrow microporosity in TACM-HOF.

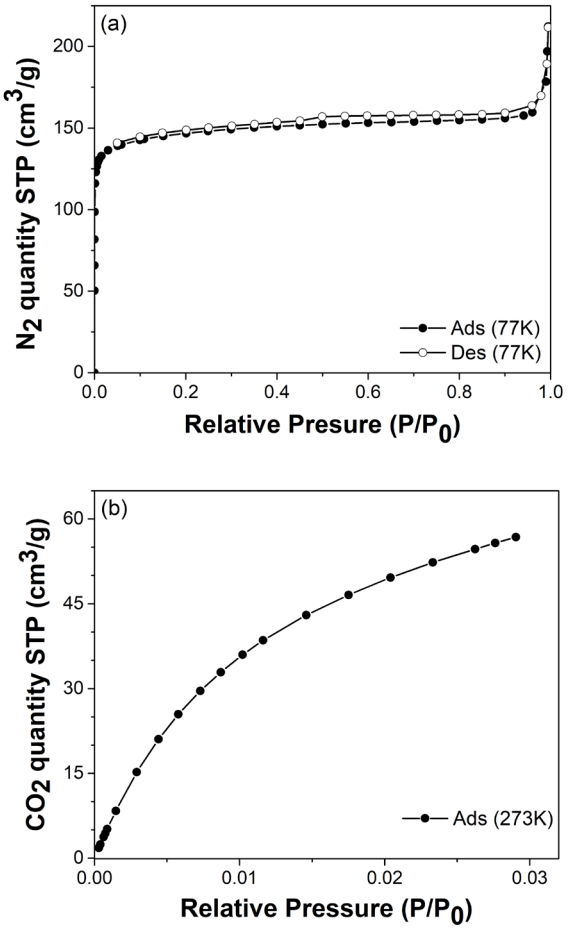

Figure 7. (a) N_2 isotherm of TACM-HOF at 77 K until 1 bar. (b) Subatmospheric CO_2 isotherm at 273 K.

The textural features were also analyzed through the contribution of different pore sizes to the pore volume of TACM-HOM (Table S3),[31] concluding that the microporosity of the material expressed as volume of liquid (0.22 cm^3g^{-1}) is almost exclusively attributable to pores in the range below 0.7 nm. This fact also supports the idea that N_2 at 77 K may experience some diffusional problems[28] when accessing the porosity of TACM-HOF, which behaves as a molecular sieve.

Additionally, density functional theory (DFT) has been used to gain a deeper understanding of the pore size distribution. Figure 8 shows both CO_2 at 273K and N_2 at 77K DFT pore size distributions for material TACM-HOF. The N_2 adsorption at 77 K by TACM-HOF best fitted to a carbon-based model, namely the quenched solid density functional theory (QSDFT) with slit/cylindrical pores, achieving a fitting error of only 0.19% on the adsorption branch.[32] The N_2 at 77K DFT analysis shows that the most frequent pore size is about 0.57 nm in diameter, with another node close to 0.97 nm. Analogously, the fitting of a non-local density functional theory (NLDFT) method to the CO_2 adsorption data at 273 K for carbon sorbent yields a pore size distribution showing that narrow micropores in TACM-HOF are between 0.4 to 0.7 nm with a most frequent diameter of 0.50 nm and a node at 0.82 nm. It is worth highlighting how the most frequent pore size obtained by DFT analysis of the gas adsorption isotherms is in good agreement with the accessible pore dimensions (0.49–0.66 nm) previously discussed for the X-ray diffraction structure (Figure 3a). Moreover, the total pore volume expressed as a liquid (0.25 cm^3g^{-1}) assessed from DFT analysis of N_2 adsorption at 77 K matches the value of 0.25 cm^3g^{-1} calculated from the N_2 isotherm at P/P_0 of 0.96.

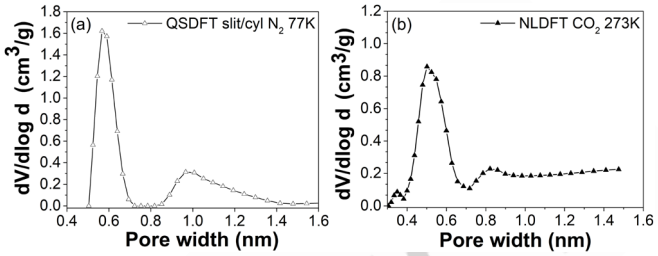

Figure 8. DFT pore size distribution (PSD) of TACM-HOF obtained from subatmospheric N_2 isotherm at 77 K (a) for a carbon model sorbent.and CO_2 isotherm at 273 K (b).

To further investigate the gas storage ability of the TACM-HOF, high pressure isotherms (up to 20 bar) for CO_2, CH_4 and H_2 at 273 K, 283 K and 298 K were collected (Figure 9 and Table 1). CO_2 isotherms show high gas uptake at low pressures presumably due to a more favorable attractive interaction between the adsorbate and the adsorbent. A less pronounced slope manifests at pressures higher than 5 bar, reaching a CO_2 capacity of 127 cm^3g^{-1} of gas STP (0.25 gg^{-1}) at 273 K and 20 bar, which is comparable to some other good HOF-based adsorbents (Table S5).[33] For the sake of comparison, CO_2 adsorption up to 1 bar at 273 K corresponded to 57 cm^3g^{-1} of gas STP (0.11 gg^{-1}). It is worth noticing that these values are quite significant for a material with a moderate surface area, being comparable to some other HOFs measured under similar conditions but with larger BET surfaces (Table S5).[15, 33b, 34] Concerning CH_4 adsorption, type I isotherms were also obtained with a gas uptake of 73 cm^3g^{-1} of gas STP (0.05 gg^{-1}) at 273 K and 20 bar. A CH_4 capacity of 24 cm^3g^{-1} (0.02 gg^{-1}) was determined at 1 bar and 273 K. In the case of hydrogen isotherms, linear plots were observed under the abovementioned conditions of temperature and pressure.

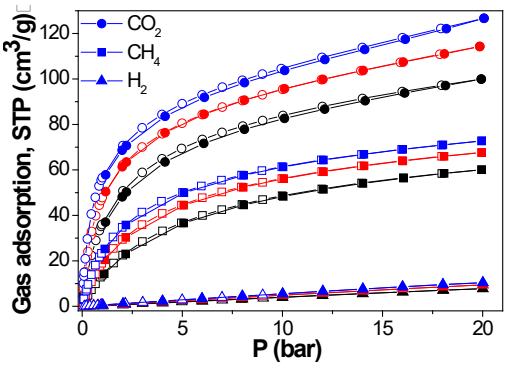

Figure 9. Sorption isotherms for ● CO_2, ■ CH_4 and ▲ H_2 at 298K (black plots), 283 K (red plots), and 273 K (blue plots) up to 20 bar. Adsoption (filled symbols) and desorption (empty symbols).

In agreement with these results, TACM-HOF evidences a clear selectivity towards CO_2 adsorption. This was further confirmed by the isosteric heats of adsorption (Table 1) determined from the isotherms recorded at different temperatures up to 20 bar using the Van't Hoff equation[35] and extrapolating the values at zero coverage by linear regression of the data (Figure S15). The adsorption enthalpy at low coverage calculated for CO_2 is 27.4 kJ/mol and can be interpreted as quite high compared to other reported HOFs (Table S5),[16, 33a] corroborating the strength of the interaction between the CO_2 molecules and the microporous organic material. A better affinity of TACM-HOF for CO_2 over CH_4 and H_2, and CH_4 over H_2 can be inferred from the isosteric heats of adsorption at zero coverage.

Table 1. TACM-HOF adsorption capacity at 20 bar and isosteric heat of adsorption.

	Gas uptake at 273 K (cm^3g^{-1} gas STP)	Gas uptake at 283 K (cm^3g^{-1} gas STP)	Gas uptake at 298 K (cm^3g^{-1} gas STP)	Q_{st} (kJ/mol)
CO_2	127	114	100	27.4
CH_4	73	68	60	21.4
H_2	10	9	8	8.3

The observed favorable CO_2 uptake can be related to different aspects: i) dispersion forces in carbon dioxide are stronger than in methane, due to the quadrupole moment present in CO_2,[36] resulting also in stronger dispersion forces between CO_2 and the surface of the adsorbent; ii) the adequacy of the size of the channels in the interpenetrated network to accommodate the CO_2 molecule, with a kinetic diameter of 0.33 nm and a linear geometry, compared to methane, with a kinetic diameter of 0.38 nm and iii) the presence of a suitable surface chemistry.[37]

The selectivity towards CO_2 adsorption was assessed by Grand Canonical Monte Carlo (GCMC) simulations of guest gases in TACM-HOF as implemented in the RASPA2 program (see the Supporting Information for computational details).[38] The most probable region to find an adsorbed CO_2 molecule is predicted in the central part of the framework cavity, displaying a helical-like probability distribution throughout the pore channel (Figure 10a,b). A similar distribution is predicted for CH_4; however, with a high-probability region that is thinner and bulgier (Figure S20). Based on the Monte Carlo results, we carried out geometry optimizations of different gas-adsorbed configurations using ab-initio density functional theory by means of the FHI-aims software (PBEsol/light-tier 1 level including van der Waals corrections).[39] Periodic calculations confirm the preference of the guest molecules for the middle region of the helical pore channel, as predicted by the GCMC density profiles (Figure S21 and S22). Interaction energies as large as −0.326 eV were calculated for CO_2, whereas a smaller value of −0.280 eV was obtained for CH_4. Analysis of these energies and the dispersion-uncorrected results suggests that the larger stabilization for CO_2 stems from a more electrostatic nature of the interaction with the framework. For the minimum-energy configuration, the CO_2 molecule presents short distances of 3.76 Å to the closest aromatic ring and 3.23 Å to the closest aromatic hydrogen atom, evidencing the presence of π–π interactions and O···H contacts, respectively (Figure 10c). Short distances are also predicted for CH_4, in this case based on CH···π and CH···HC interactions (Figure S23). The non-covalent interaction (NCI) index in the periodic systems was calculated as implemented in Critic2,[40] indicating in both gas molecules the presence of large NCI surfaces due to the weak van der Waals attractive forces with the HOF (see Figure 10c for CO_2 and Figure S23 for CH_4).

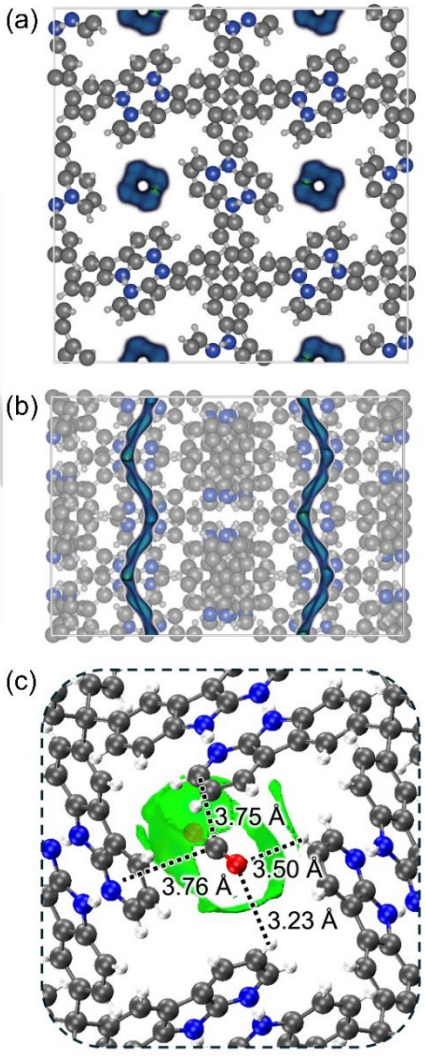

Figure 10. (a) Top view and (b) side view of the center-of-mass probability density map for CO_2 adsorbed in TACM-HOF obtained from the GCMC simulation. (c) Non-covalent interaction isosurface calculated at reduced density gradient s = 0.75 au of a CO_2 molecule in the TACM-HOF framework. Relevant distances between the gas molecule and the framework are indicated.

Concerning the adsorption selectivity of TACM-HOF for binary gas mixtures, this was calculated based on the ideal adsorbed solution theory (IAST)[41] by using the individual high pressure isotherms collected for CO_2, CH_4 and H_2 at 298 K. Different

models were tested to find the best fitting for each isotherm and spreading pressure (π*) curve (Figures S15-S17). The best fitting models were "Dual site Langmuir" for carbon dioxide, "Toth" for methane and "Langmuir" for hydrogen. Focusing on the case of the CO_2/CH_4 mixtures at different ratios (15/85, 50/50 and 85/15), a very consistent molar selectivity, 4.2–4.3, was calculated in the whole range of partial pressures for a system at atmospheric pressure (Figure S16). Additionally, TACM-HOF presents a higher affinity for CO_2 and CH_4 over H_2 as demonstrated by the CO_2/H_2 selectivity, ranging from 164 to 136, and the CH_4/H_2 selectivity, ranging between 48 and 41 (Figure S17 and S18).

The adsorption selectivity plays a critical role in the technology of gas separation. Within this context, organic frameworks have proved their utility as fillers in mixed-matrix membranes.[38] In particular, the separation of CO_2/CH_4 gas mixtures is a key challenge for the energy sector and is essential for the efficient upgrading of natural gas and biogas. For that purpose, the separation of CO_2 and CH_4 was investigated at room temperature in a fixed-bed reactor by feeding a gas mixture of 10% CO_2 + 10% CH_4 + 80 % He, and the preferential retention of CO_2 was confirmed in both the adsorption and the desorption stages (Figure 11). It can be noticed that CH_4 reaches its maximum concentration at about 20 minutes from the initial contact of the gas mixture with the material while CO_2 reaches the same concentration at the outlet of the reactor at about 40 minutes, showing that CO_2 is more strongly retained in the material than CH_4. Something similar is detected in the desorption stage even though the process is faster (11 minutes for CH_4 and 25 minutes for CO_2). The same aliquot of sample was used in different gas separation experiments (Figure S30) showing no sign of decline in the separation capacity.

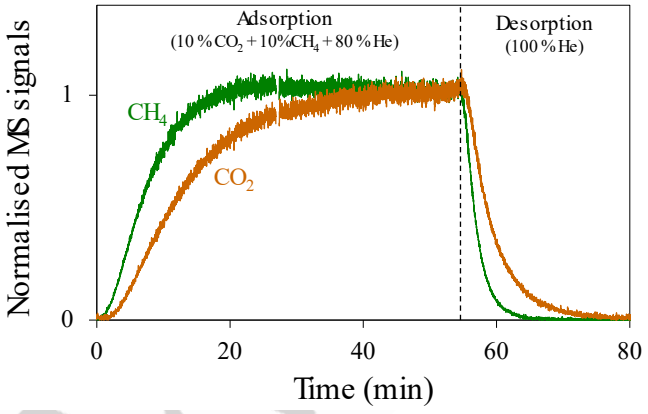

Figure 11. CO_2 and CH_4 separation experiments followed by mass spectrometry (MS). Experimental conditions: 180 mg of TACM-HOF, total gas flow 3 mL·min^{-1}, 298 K.

Due to the current interest in hydrogen as a potential alternative energy source,[42] the development of hydrogen production, transport and storage represent crucial goals. MOFs and COFs have greatly contributed to the discovery of innovative porous materials for hydrogen storage purposes in the last few years.[43] Nevertheless, due to the more recent advent of HOFs and the possible issues related to their purely non-covalent organic nature, there is a scarcity of reports about hydrogen adsorption in this type of materials.[8, 15, 44] Consequently, based on the previously discussed narrow microporosity of TACM-HOF, the isotherm for hydrogen uptake at 77 K and 1 bar was measured, showing a type I profile with a pronounced adsorption at low pressures (Figure S19). Under these conditions, a hydrogen capacity of 136 cm^{3}g^{-1} of gas STP (1.2 wt. %) was reached. Although this adsorption is far from the U. S. Department of Energy (DOE) targets for hydrogen storage[45] and from state-of-the art MOF-based materials,[46] it is worth highlighting that ii stands among the best reported for HOFs (Table S5). Therefore, the appropriate design of supramolecular frameworks could also contribute to the progress of materials for gas storage.[47]

All the discussed applications of porous organic frameworks necessarily require highly stable materials. In this respect, one of the most remarkable aspects of the TACM-HOF structure is its robustness. Even though the framework is essentially held up by non-covalent interactions, this material remains unchanged after the repeated measurement of all the isotherms up to 20 bar with the same aliquote of TACM-HOF (Figure 12). No sign of structure collapse has been found, as revealed by X-ray diffraction analysis after high pressure gas adsorption experiments that demonstrate the structural integrity of the crystalline material.

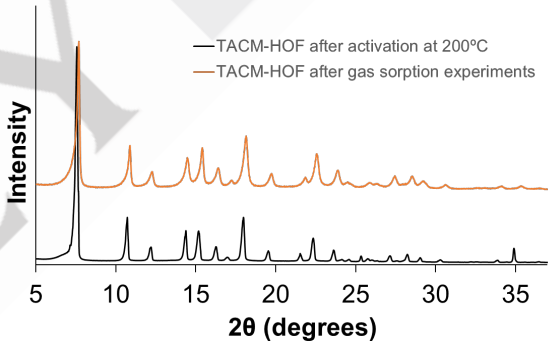

Figure 12. Comparison of powder X-ray diffraction before (black plot) and after (orange plot) gas sorption experiments. The diffraction peak at ~35° in the black plot corresponds to the alumina sample holder.

Conclusion

The synthesis of a suitable tecton for hydrogen-bonded organic frameworks, namely TACM-HOF, has been reported, incorporating 7-azaindole as an innovative rigid hydrogen-bonding building block. The tetrahedral structure of TACM self-assembles to spontaneously form a five-fold diamonoid 3D-interpenetrated network that constitutes a microporous crystalline material with unidirectional channels. These structural features bestow the HOF an extraordinary thermal robustness (Td > 515 ºC) within the context of supramolecular organic frameworks. The gas adsorption experiments have revealed a high capacity for the CO_2 uptake, showing selectivity over CH_4 adsorption. Interestingly, the microporous structure of TACM-HOF has achieved a reasonable adsorption capacity for H_2 at 77 K with a fast gas uptake at reduced pressure. Therefore, our results show the important implication that molecular design has on the stability

and porous architecture of supramolecular organic frameworks, and the adequacy of 7-azaindole as synthon for robust hydrogen-bonding. Additionally, the adsorption properties of TACM-HOF are indicative of the potential application in the capture of a greenhouse effect pollutant such as CO_2 or in processes related to the exploitation of H_2 as alternative energy source.

Supporting Information

Synthesis and structural characterization (NMR spectra), thermal characterization (TGA and DSC), single-crystal X-ray diffraction, powder X-ray diffraction, transmission electron microscopy, gas sorption experiments.

Acknowledgements

Authors acknowledge the financial support from the Ministry of Science and Innovation (PID2021-122734OB-I00; RED2022-134939-T), Fundación Séneca-Agencia de Ciencia y Tecnología de la Región de Murcia (Project 22058/PI/22), Projects MFA/2022/036 by MCIN with funding from European Union NextGeneration EU (PRTR-C17.I1) and by Generalitat Valenciana, PID2020-119748GA-I00 funded by MCIN, and aid EQC2019-006482-P with funding from European Union and MCIN (AEI/10.13039/501100011033).

Keywords: hydrogen-bonded organic framework • HOF • self-assembly • gas sorption

[1] O. M. Yaghi, M. J. Kalmutzki, C. S. Diercks, *Introduction to Reticular Chemistry: Metal - Organic Frameworks and Covalent Organic Frameworks*, Wiley - VCH Verlag GmbH & Co. KGaA, **2019**.

[2] a) H.-C. J. Zhou, S. Kitagawa, *Chem. Soc. Rev.* **2014**, *43*, 5415-5418; b) H. Furukawa, K. E. Cordova, M. O'Keeffe, O. M. Yaghi, *Science* **2013**, *341*, 1230444.

[3] a) K. Geng, T. He, R. Liu, S. Dalapati, K. T. Tan, Z. Li, S. Tao, Y. Gong, Q. Jiang, D. Jiang, *Chem. Rev.* **2020**, *120*, 8814-8933; b) S. Kandambeth, K. Dey, R. Banerjee, *J. Am. Chem. Soc.* **2019**, *141*, 1807-1822.

[4] a) Z. Zhang, Y. Ye, S. Xiang, B. Chen, *Acc. Chem. Res.* **2022**, *55*, 3752-3766; b) Z.-J. Lin, S. A. R. Mahammed, T.-F. Liu, R. Cao, *ACS Cent. Sci.* **2022**, *8*, 1589-1608; c) R.-B. Lin, B. Chen, *Chem* **2022**, *8*, 2114-2135; d) L. Chen, B. Zhang, L. Chen, H. Liu, Y. Hu, S. Qiao, *Mater. Adv.* **2022**, *3*, 3680-3708; e) B. Wang, R.-B. Lin, Z. Zhang, S. Xiang, B. Chen, *J. Am. Chem. Soc.* **2020**, *142*, 14399-14416; f) P. Li, M. R. Ryder, J. F. Stoddart, *Acc. Mater. Res.* **2020**, *1*, 77-87.

[5] I. Hisaki, C. Xin, K. Takahashi, T. Nakamura, *Angew. Chem. Int. Ed.* **2019**, *58*, 11160-11170.

[6] X. Song, Y. Wang, C. Wang, D. Wang, G. Zhuang, K. O. Kirlikovali, P. Li, O. K. Farha, *J. Am. Chem. Soc.* **2022**, *144*, 10663-10687.

[7] R.-B. Lin, Y. He, P. Li, H. Wang, W. Zhou, B. Chen, *Chem. Soc. Rev.* **2019**, *48*, 1362-1389.

[8] C. A. Zentner, H. W. H. Lai, J. T. Greenfield, R. A. Wiscons, M. Zeller, C. F. Campana, O. Talu, S. A. FitzGerald, J. L. C. Rowsell, *Chem. Commun.* **2015**, *51*, 11642-11645.

[9] K. Ma, P. Li, J. H. Xin, Y. Chen, Z. Chen, S. Goswami, X. Liu, S. Kato, H. Chen, X. Zhang, J. Bai, M. C. Wasson, R. R. Maldonado, R. Q. Snurr, O. K. Farha, *Cell Rep. Phys. Sci.* **2020**, *1*, 100024.

[10] I. Hisaki, N. Ikenaka, N. Tohnai, M. Miyata, *Chem. Commun.* **2016**, *52*, 300-303.

[11] I. Hisaki, Y. Suzuki, E. Gomez, Q. Ji, N. Tohnai, T. Nakamura, A. Douhal, *J. Am. Chem. Soc.* **2019**, *141*, 2111-2121.

[12] W. Yang, F. Yang, T.-L. Hu, S. C. King, H. Wang, H. Wu, W. Zhou, J.-R. Li, H. D. Arman, B. Chen, *Cryst. Growth Des.* **2016**, *16*, 5831-5835.

[13] H. Wang, B. Li, H. Wu, T.-L. Hu, Z. Yao, W. Zhou, S. Xiang, B. Chen, *J. Am. Chem. Soc.* **2015**, *137*, 9963-9970.

[14] M. Vicent-Morales, M. Esteve-Rochina, J. Calbo, E. Ortí, I. J. Vitórica-Yrezábal, G. Mínguez Espallargas, *J. Am. Chem. Soc.* **2022**, *144*, 9074-9082.

[15] M. Mastalerz, I. M. Oppel, *Angew. Chem. Int. Ed.* **2012**, *51*, 5252-5255.

[16] I. Bassanetti, S. Bracco, A. Comotti, M. Negroni, C. Bezuidenhout, S. Canossa, P. P. Mazzeo, L. Marchió, P. Sozzani, *J. Mater. Chem. A* **2018**, *6*, 14231-14239.

[17] a) X. Zhang, J.-X. Wang, L. Li, J. Pei, R. Krishna, H. Wu, W. Zhou, G. Qian, B. Chen, B. Li, *Angew. Chem. Int. Ed.* **2021**, *60*, 10304-10310; b) O. Ermer, *J. Am. Chem. Soc.* **1988**, *110*, 3747-3754; c) D. J. Duchamp, R. E. Marsh, *Acta Crystallogr. Sect. B: Struct. Sci.* **1969**, *25*, 5-19.

[18] M. Simard, D. Su, J. D. Wuest, *J. Am. Chem. Soc.* **1991**, *113*, 4696-4698.

[19] a) P. Li, Y. He, H. D. Arman, R. Krishna, H. Wang, L. Weng, B. Chen, *Chem. Commun.* **2014**, *50*, 13081-13084; b) P. Brunet, M. Simard, J. D. Wuest, *J. Am. Chem. Soc.* **1997**, *119*, 2737-2738.

[20] a) D.-D. Zhou, Y.-T. Xu, R.-B. Lin, Z.-W. Mo, W.-X. Zhang, J.-P. Zhang, *Chem. Commun.* **2016**, *52*, 4991-4994; b) T.-H. Chen, I. Popov, W. Kaveevivitchai, Y.-C. Chuang, Y.-S. Chen, O. Daugulis, A. J. Jacobson, O. Š. Miljanić, *Nat. Commun.* **2014**, *5*, 5131.

[21] a) B. Yu, L. Li, S. Liu, H. Wang, H. Liu, C. Lin, C. Liu, H. Wu, W. Zhou, X. Li, T. Wang, B. Chen, J. Jiang, *Angew. Chem. Int. Ed.* **2021**, *60*, 8983-8989; b) Y.-L. Wu, N. E. Horwitz, K.-S. Chen, D. A. Gomez-Gualdron, N. S. Luu, L. Ma, T. C. Wang, M. C. Hersam, J. T. Hupp, O. K. Farha, R. Q. Snurr, M. R. Wasielewski, *Nat. Chem.* **2017**, *9*, 466-472.

[22] a) P. Gómez, J. Wang, M. Más-Montoya, D. Bautista, C. H. L. Weijtens, D. Curiel, R. A. J. Janssen, *Solar RRL* **2021**, *5*, 2100454; b) P. Gómez, S. Georgakopoulos, M. Más-Montoya, J. Cerdá, J. Pérez, E. Ortí, J. Aragó, D. Curiel, *ACS Appl. Mater. Interfaces* **2021**, *13*, 8620-8630; c) P. Gómez, J. Cerdá, M. Más-Montoya, S. Georgakopoulos, I. da Silva, A. García, E. Ortí, J. Aragó, D. Curiel, *J. Mater. Chem. C* **2021**, *9*, 10819-10829; d) M. Más-Montoya, P. Gómez, D. Curiel, I. da Silva, J. Wang, R. A. J. Janssen, *Chem. Eur. J.* **2020**, *26*, 10276-10282.

[23] a) I. G. Sonsona, M. Carrera, M. Más-Montoya, R. S. Sánchez, P. Serafini, E. M. Barea, I. Mora-Seró, D. Curiel, *ACS Appl. Mater. Interfaces* **2023**, *15*, 22310-22319; b) L. M. Rodríguez, P. Gómez, M. Más-Montoya, J. Abad, A. Tárraga, J. I. Cerdá, J. Méndez, D. Curiel, *Angew. Chem. Int. Ed.* **2021**, *60*, 1782-1788.

[24] P. Ganesan, X. Yang, J. Loos, T. J. Savenije, R. D. Abellon, H. Zuilhof, E. J. R. Sudhölter, *J. Am. Chem. Soc.* **2005**, *127*, 14530-14531.

[25] L. J. Barbour, *Chem. Commun.* **2006**, 1163-1168.

[26] C. F. Macrae, I. Sovago, S. J. Cottrell, P. T. A. Galek, P. McCabe, E. Pidcock, M. Platings, G. P. Shields, J. S. Stevens, M. Towler, P. A. Wood, *J. Appl. Crystallogr.* **2020**, *53*, 226-235.

[27] Q. Chen, C. Dwyer, G. Sheng, C. Zhu, X. Li, C. Zheng, Y. Zhu, *Adv. Mater.* **2020**, *32*, 1907619.

[28] M. Thommes, K. Kaneko, A. V. Neimark, J. P. Olivier, F. Rodriguez-Reinoso, J. Rouquerol, K. S. W. Sing, *Pure Appl. Chem.* **2015**, *87*, 1051-1069.

[29] The presence of certain macropores cannot be ruled out with the available data (BJH pore size distribution on the equilibrium branch informs of pore sizes up to 300 nm in diameter, Figure S13).

[30] D. Lozano-Castelló, D. Cazorla-Amorós, A. Linares-Solano, *Carbon* **2004**, *42*, 1233-1242.

[31] Chemistry and Physics of Carbon, P.L. Walker(Ed.),1st ed., Vol. 21, Dekker, 1988, Ch1.

[32] All the models available in Quadrawin Software (Anton-Paar, QuantaTec) for N_2 adsorption at 77 K on carbon materials were tested for TACM-HOF between P/P_0 10^{-7} to 0.96, including NLDFT and QSDFT with slit, cylindrical, spherical pores or combinations of them, on adsorption or equilibrium (desorption) branches.

[33] a) J. Lü, C. Perez-Krap, F. Trousselet, Y. Yan, N. H. Alsmail, B. Karadeniz, N. M. Jacques, W. Lewis, A. J. Blake, F.-X. Coudert, R. Cao, M. Schröder, *Cryst. Growth Des.* **2018**, *18*, 2555-2562; b) J. Lü, C. Perez-Krap, M. Suyetin, N. H. Alsmail, Y. Yan, S. Yang, W. Lewis, E.

Bichoutskaia, C. C. Tang, A. J. Blake, R. Cao, M. Schröder, *J. Am. Chem. Soc.* **2014**, *136*, 12828-12831.

[34] P. Li, P. Li, M. R. Ryder, Z. Liu, C. L. Stern, O. K. Farha, J. F. Stoddart, *Angew. Chem. Int. Ed.* **2019**, *58*, 1664-1669.

[35] a) P. L. Llewellyn, G. Maurin, in *Stud. Surf. Sci. Catal., Vol. 168* (Eds.: J. Čejka, H. van Bekkum, A. Corma, F. Schüth), Elsevier, **2007**, pp. 555-XVI; b) H. H. Rowley, W. B. Innes, *Proc. Iowa Acad. Sci.* **1940**, *47*, 165-170.

[36] a) G. M. Meconi, R. Zangi, *Phys. Chem. Chem. Phys.* **2020**, *22*, 21031-21041; b) N. Álvarez-Gutiérrez, M. V. Gil, F. Rubiera, C. Pevida, *Fuel Process. Technol.* **2016**, *142*, 361-369.

[37] X. Peng, S. K. Jain, J. K. Singh, *J. Phys. Chem. C* **2017**, *121*, 13457-13473.

[38] a) D. Dubbeldam, S. Calero, D. E. Ellis, R. Q. Snurr, *Mol. Simul.* **2016**, *42*, 81-101; b) D. Dubbeldam, A. Torres-Knoop, K. S. Walton, *Mol. Simul.* **2013**, *39*, 1253-1292.

[39] V. Blum, R. Gehrke, F. Hanke, P. Havu, V. Havu, X. Ren, K. Reuter, M. Scheffler, *Comput. Phys. Commun.* **2009**, *180*, 2175-2196.

[40] A. Otero-de-la-Roza, E. R. Johnson, V. Luaña, *Comput. Phys. Commun.* **2014**, *185*, 1007-1018.

[41] A. L. Myers, J. M. Prausnitz, *AIChE J.* **1965**, *11*, 121-127.

[42] C. Kim, S. H. Cho, S. M. Cho, Y. Na, S. Kim, D. K. Kim, *Int. J. Hydrogen Energy* **2023**, *48*, 1701-1716.

[43] a) D. Zhao, X. Wang, L. Yue, Y. He, B. Chen, *Chem. Commun.* **2022**, *58*, 11059-11078; b) M. P. Suh, H. J. Park, T. K. Prasad, D.-W. Lim, *Chem. Rev.* **2012**, *112*, 782-835; c) J. Sculley, D. Yuan, H.-C. Zhou, *Energy & Environmental Science* **2011**, *4*, 2721-2735.

[44] K. J. Msayib, D. Book, P. M. Budd, N. Chaukura, K. D. M. Harris, M. Helliwell, S. Tedds, A. Walton, J. E. Warren, M. Xu, N. B. McKeown, *Angew. Chem. Int. Ed.* **2009**, *48*, 3273-3277.

[45] DOE Technical Targets for Onboard Hydrogen Storage for Light-Duty Vehicles. https://www.energy.gov/eere/fuelcells/doe-technical-targets-onboard-hydrogen-storage-light-duty-vehicles

[46] a) D. E. Jaramillo, H. Z. H. Jiang, H. A. Evans, R. Chakraborty, H. Furukawa, C. M. Brown, M. Head-Gordon, J. R. Long, *J. Am. Chem. Soc.* **2021**, *143*, 6248-6256; b) M. T. Kapelewski, T. Runčevski, J. D. Tarver, H. Z. H. Jiang, K. E. Hurst, P. A. Parilla, A. Ayala, T. Gennett, S. A. FitzGerald, C. M. Brown, J. R. Long, *Chem. Mater.* **2018**, *30*, 8179-8189.

[47] Z. Chen, K. O. Kirlikovali, K. B. Idrees, M. C. Wasson, O. K. Farha, *Chem* **2022**, *8*, 693-716.

Entry for the Table of Contents

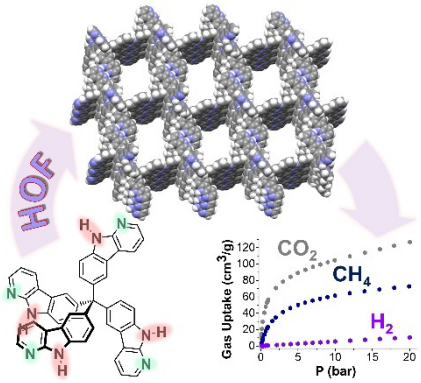

A preorganized tetrapodal building block, incorporating α-carboline units, self-assembles to form a 3D hydrogen-bonded organic framework (HOF). The expanded hydrogen bonding between the heteroaromatic substructures, along with intermolecular π-π interactions, spontaneously build up an interpenetrated architecture that bestows an extraordinary robustness to the microporous crystalline material, showing a good selectivity for CO_2 adsorption.